Session 1P3b
Remote Sensing and Imaging

On the Analysis of Geophysical Networks from Multiscale DEMs

L. T. Tay, **B. S. D. Sagar**, **and H. T. Chuah**
Multimedia University, Malaysia

A lot of information can be extracted from digital elevation models (DEMs) and it offers scientists with invaluable information in terrain characterization. Regions with varied degrees of concavity and convexity represent various degrees of terrain complexities. These complexities explain various physiographic and geomorphic processes. The abstract structures of concave and convex zones represent the valley and ridge connectivity networks respectively. These two unique topological networks have immense use in characterizing the surficial terrain quantitatively via morphometry, hypsometry, allometric scaling and granulometry. The main objective of this paper is to present a method based on morphological transformations in extracting the network and fractal techniques in terrain characterization. We analyze the intereferometrically derived DEM of Cameron Highlands and Tioman region of Malaysia. Cameron Highlands region comprises a series of mountain stations at altitudes between 500 m and 1300 m whereas Tioman region is parts of an Island with altitude ranges from sea level to 500 m.

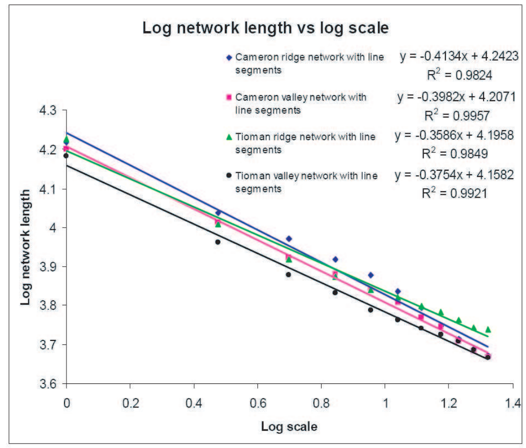

Figure 1.

We employ multiscale nonlinear morphological transformations to generate DEMs at multiple resolutions and to extract channel and ridge networks from these multiscale DEMs. We provide a simple scaling law from the relationship shown by considering the lengths of unique networks derived from multiscale DEMs as functions of radius of the structuring element. It is shown as a simple resolution-independent power-law dimension in the form of $l \sim r^{\alpha}$, where l and r denote length of network at different scale and radius of structuring element respectively. α as the scaling exponent, is the fractal dimension of network. This relationship depict that similar trends have been followed for both ridge and valley connectivity networks and describes the scaling properties of the terrain where the density of the networks decreases as the resolution decreases. The plot of network lengths as functions of radius of structuring element is in logarithm values (figure below). The gradients of best fit lines of these plots indicate that the rate of change in the lengths of the networks, across multiple resolutions. The complexities and intricacies of valley and ridge network change with various types of topography, therefore network length is considered as an important parameter for complex geometry of valley and ridge. We prove that hilly terrain (Cameron Highland region) possesses higher value of exponent as compared to non-hilly terrain (Tioman region). The reason is the rate of change in elevation of hilly terrain across resolution is higher than non-hilly terrain. Relatively, the network intricacies will change more rapidly for hilly terrain. Further analyses of these two networks provide the morphologies of convex ones and hillslopes. The length criterion and fractal dimensions of networks can be used as a powerful criterion for the classification among sub-basins in a large basin. Basins with different topography structure have different network geometry and densities. Emerging river network patterns can be considered to relate with basic underlying physical mechanisms involved in the formation of landscapes of varied complexities. The differences will be reflected by the fractal dimension as this exponent is computed based on network densities across multiple scales.

Buried Cylinders Geometric Parameters Measurement by Means of GPR

B. A. Yufryakov and O. N. Linnikov
Scientific and Technical Centre of System Modeling, Russia

Abstract—Interactive technique that measures geometric parameters of buried cylinders in a homogeneous medium with unknown velocity of signal propagation is developed. After 3D GPR data processing, the velocity of signal propagation is estimated; radius, length and position of the cylinder are measured. Experimental data obtained by GPR "Defectoscope" are given.

1. Introduction

In paper [1] the hyperbola-fitting technique of radius estimation for subsurface cylindrical objects is presented. For that a direct least-square method for fitting hyperbola is used. Authors of paper [1] supposed that the propagation velocity is known or it can be estimated beforehand via finding a hyperbola resulting from a point reflector within the radarogram. In paper [2] they solved the questions of improving the accuracy of the interpretation of the radar returns reflected from buried cylinders by taking into account the influence of cylinder's orientation and electromagnetic radiation pattern of the antennas.

In [3] two-dimensional data obtained from orthogonal sounding of cylinders are analyzed. It is shown that the generalized Hough method can be used to measure buried pipe diameters from radar measurements and the velocity determination is best made independently from a point-like source at similar depth.

In this paper the interactive technique of 3D-data processing which allows us to estimate simultaneously signal propagation velocity in the medium and cylindrical objects parameters (orientation, radius, length and depth of occurrence) is proposed. Operator participation in data processing allows one to smooth reflected signals registration errors.

The technique is based on the frontal method of GPR 3D-data interpretation [4]. This method selects from the whole bulk of GPR data the first arrival of wave fronts from the recorded signals reflected from objects. These selected surfaces will be referred to as frontal hodographs.

This paper is development of the work in [5].

2. Measurement Technique

The technique proposed was developed during the creation of GPR data processing software of GPR "Defectoscope", designed for inspection of buildings [6]. The scan zone of this GPR is a rectangular area in the XY plane, and Z axis is directed to the probed medium. We will call the geometrical space with coordinate system XYZ as object space. During the results registration at any scanning point the value of reflected signal is fixed at discrete time moments at time axis T. This data array we will call the signal space or data cube. In the signal space by means of software tools, it is possible to select the surfaces of frontal hodographs as a function of time delay τ from antenna system coordinates (X, Y).

In Fig. 1, a cylinder with arbitrary orientation with respect to scanning plane is shown. Denote cylinder radius as r. Angle of inclination with respect to scanning plane XY of cylinder axis is denoted as φ; its projection to the plane XY intercepts X axis at angle θ. Let us carry out a parallel shift of axes X and Y into an arbitrary point O belonging to the cylinder axis projection into scanning plane. In Fig. 1 such shift has been made. Cylinder axis intersects the scanning plane at a point with coordinates (CX, CY). The distance between point O and cylinder axis are denoted as h_0. This distance equals the length of the perpendicular drawn from this point to the cylinder axis.

Let us consider this perpendicular as vector $\vec{h}=\{X_0, Y_0, Z_0\}$, where (X_0, Y_0, Z_0) are Cartesian coordinates of the perpendicular base, they are:

$$X_0 = -h_0 \sin\varphi \cos\theta, \quad Y_0 = -h_0 \sin\varphi \sin\theta, \quad Z_0 = h_0 \cos\varphi\,.$$

Let us introduce the unit vector $\vec{e}_C=\{l_0, m_0, n_0\}$ directed from the considered perpendicular base along the cylinder axis in increasing depth. Coordinates of this vector are:

$$l_0 = \cos\varphi \cos\theta, \quad m_0 = \cos\varphi \sin\theta, \quad n_0 = \sin\varphi\,.$$

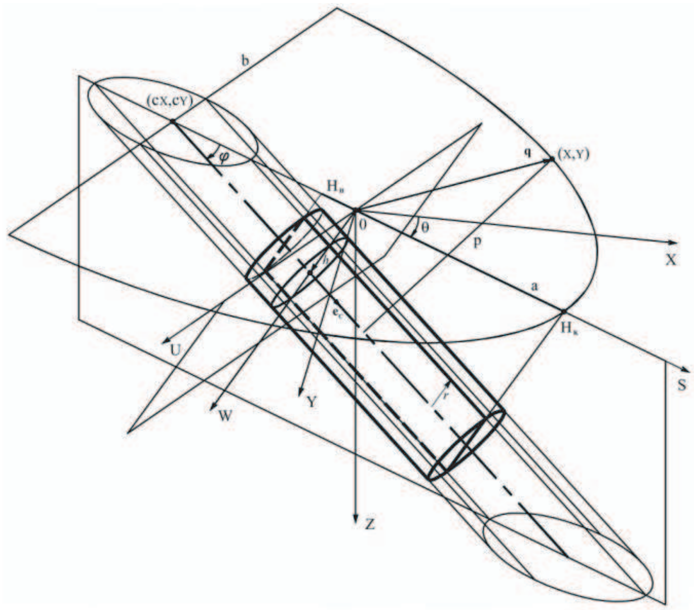

Figure 1: Geometry of data acquisition above an arbitrary located cylinder.

Then distance $p(X,Y)$ from arbitrary point (X,Y) of scanning plane to cylinder axis equals:

$$p(X,Y) = \frac{\left|\left[\vec{q}-\vec{h},\vec{e}_C\right]\right|}{|\vec{e}_C|}$$

where $\vec{q}=\{X,\ Y,\ 0\}$, – radius-vector of the point (X,Y), $\left[\vec{q}-\vec{h},\vec{e}_C\right]$ –vector product of vectors $\vec{q}-\vec{h}=\{X-X_0, Y-Y_0, -Z_0\}$ and $\vec{e}_C$, modulus means the length of the vector, i.e., $\left|\vec{h}\right| = h_0$.

Hence

$$p^2(X,Y) = [(Y-Y_0)n_0 + m_0 z_0]^2 + [(X-X_0)n_0 + l_0 z_0]^2 + [(X-X_0)m_0 - (Y-Y_0)l_0]^2.$$

Substituting appropriate coordinates and simplifying, we obtain:

$$p^2(X,Y) = (X\sin\varphi + h_0\cos\theta)^2 + (Y\sin\varphi + h_0\sin\theta)^2 + \cos^2\varphi(X\sin\theta - Y\cos\theta)^2$$

Point (X,Y) belongs to the arc of ellipse with major semiaxis a and minor semiaxis b (see Fig. 1), where

$$a = p(X,Y)/\sin\varphi \quad \text{and} \quad \mathrm{b = p(X,Y)}.$$

This ellipse is very interesting. Coordinates of ellipse center are (CX, CY). The minor semiaxis b equals the distance from any point of ellipse to cylinder axis. The major semiaxis a is the cylinder axis projection into scanning plane. Therefore it defines angle θ. Ratio $b/a = \sin\varphi$ shows the angle inclination of cylinder axis to scanning plane.

The shortest distance $R(X,Y)$ from arbitrary point with coordinates (X,Y) at scanning plane to the cylinder surface can be derived as:

$$R(X,Y) = \sqrt{(X\sin\varphi + h_0\cos\theta)^2 + (Y\sin\varphi + h_0\sin\theta)^2 + \cos^2\varphi(X\sin\theta - Y\cos\theta)^2} - r. \tag{1}$$

Let us choose a measuring coordinate system SOU in the scanning plane which is formed by rotation of axes OX and OY by angle θ. Then OS axis will coincide with the projection of cylinder axis into the scanning plane and OU axis will be orthogonal to it. The third axis of the measuring coordinate system OW we will choose as a continuation of the perpendicular from the point O to the cylinder axis.

Then coordinates X and Y are related with measuring coordinates S and U as:

$$X = S\cos\theta - U\sin\theta \quad \text{and} \quad Y = S\sin\theta + U\cos\theta. \tag{2}$$

Section of cylinder by the UW plane is a circle with radius r and center, whose distance from point O equals h_0. For monostatic system frontal hodograph or reflections from this circle for movement along OU axis one can obtain substituting (2) into (1) with conditions $S = 0$ and $R = \frac{V\tau}{2}$:

$$\frac{V\tau}{2} = \sqrt{h_0^2 + U^2} - r.$$

Let us analyze this hyperbolic hodograph. We fix the time delay T_0 of observed hyperbola vertex at point O and delays T_1 and T_2 for arbitrary coordinates U_1 and U_2 at axis U. According to the measurement results one can obtain equations set:

$$\frac{VT_0}{2} = h_0 - r; \quad \frac{VT_1}{2} = \sqrt{h_0^2 + U_1^2} - r; \quad \frac{VT_2}{2} = \sqrt{h_0^2 + U_2^2} - r.$$

The solution is:

$$V = \frac{2}{\sqrt{T_2 - T_1}} \sqrt{\frac{U_2^2}{T_2 - T_0} - \frac{U_1^2}{T_1 - T_0}}; \tag{3}$$

$$h_0 = \frac{1}{2\sqrt{T_2 - T_1}} \frac{U_1^2(T_2 - T_0)^2 - U_2^2(T_1 - T_0)}{\sqrt{U_2^2(T_1 - T_0)^2(T_2 - T_0) - U_1^2(T_2 - T_0)^2(T_1 - T_0)}}; \tag{4}$$

$$r = h_0 - \frac{VT_0}{2}. \tag{5}$$

It should be noted that V and h_0 do not depend on T_0 but depend on differences $(T_1 - T_0)$ and $(T_2 - T_0)$. It means that signal propagation velocity and the depth of the cylinder axis could be defined unambiguously on hyperbola form independently the hyperbola position at time axis.

However, it is impossible to use (3)–(5) due to the coordinates registration errors and errors of the operator carrying out this measurements. Even little errors could lead to significant deviations of calculated V and h_0 from true values. This is a typical incorrect problem, it is advisable to solve this problem by frontal hodograph $\tau(U)$ adjustment by means of graphical tools with the best approximation of the observed data. Similar procedures are widely used in GPR for the measurement of the signal propagation velocity on reflections from point-like objects.

Approximating hyperbola form selection can be organized by software tools via adjustment of measurable parameters V, h and r according to the equations:

for monostatic system

$$\tau(U, h_0, r, V) = 2\frac{\sqrt{U^2 + h_0^2} - r}{V}; \tag{6}$$

for bistatic system with base 2d (which is parallel to X axis):

$$\tau(U, h_0, r, V) = \frac{1}{V}(\sqrt{R^2 + d^2 + 2Rd\cos\psi} + \sqrt{R^2 + d^2 - 2Rd\cos\psi}), \tag{7}$$

where $h_0 = \frac{VT_0}{2} + r$; $R = \sqrt{U^2 + h_0^2} - r$; $\cos\psi = \frac{U\sin\theta}{\sqrt{U^2 + h_0^2}}$.

Similar analysis of signal space SOT section shows that in this section frontal hodograph represents segment of the cylinder high generatrix. The slope of this segment equals the value of φ angle. Denote time delays at beginning and the end of the approximating segment as T_H and T_K respectively, and the distance between points of measurements at OS axis as D, then φ can be calculated as follows:

$$\varphi = atctg\left(\frac{V(T_K - T_H)}{2D}\right).$$

The cylinder length is $L = D\cos\varphi$.

The technique developed was realized as a software module of GPR "Defectoscope" [6]. This software was approved experimentally by sounding three parallel cylindrical objects placed into a box filled with sand. Cylinders radii were 2 cm, 0.5 cm and 4 cm. Fig. 2 shows the geometrical position of these cylinders for two soundings.

Figure 3 shows data processing results obtained from these soundings. Frame 3a shows GPR data when cylinders ware located at angle $\theta = 60°$ to X axis and angle of $\varphi = 0°$ to the scanning plane. Frame 3b

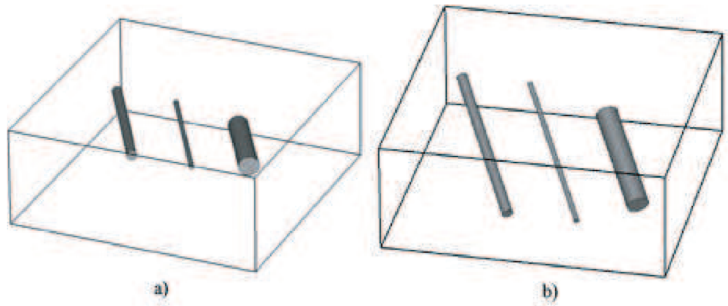

Figure 2: Cylindrical objects position in testing soundings.
(a—horizontal cylinders $\theta = 60°$ and $\varphi = 0°$, b—inclined cylinders $\theta = 60°$ and $\varphi = 30°$).

shows GPR data when $\theta = 60°$ and $\varphi = 30°$. Every frame shows control panel of the dialog window and four fragments. Two uppers fragments (1 and 2) show two vertical mutually perpendicular to each other time sections of GPR data cube. Down left fragment (3) shows a horizontal projection of data cube section which is cut in accordance with angles θ and φ. Fragment 4 is horizontal projection of data cube with signals exceeded the threshold specified by the operator.

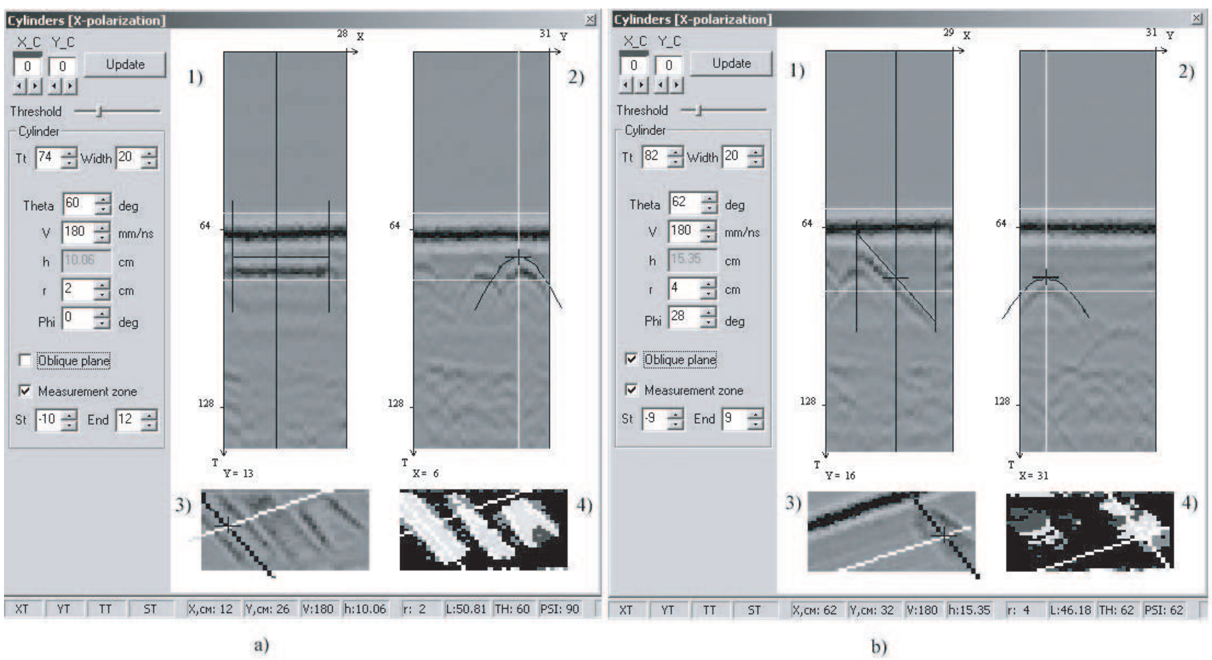

Figure 3: Measurement results of unknown parameters of medium and cylinders using GPR data. (a—horizontal cylinders $\theta = 60°$ and $\varphi = 0°$, b—inclined cylinders $\theta = 60°$ and $\varphi = 30°$, 1—vertical data cube section along S axes shown in section 3 black line, 2—vertical data cube section along U axes shown in section 3 white line, 3—section which is parallel axis of cylinder, 4—horizontal projection of data cube which show signals exceeded the threshold specified by the operator).

Consider the sequence of measurements the result of which is shown in Figs. 3(a) and 3(b). Using reflections from a cylinder it is necessary to fix a point of measurements above the axis of a cylinder (see intersection of black and white lines on fragments 3 and 4). Furthermore, an interpreter chooses the direction along the axis of cylinder using reflections in horizontal section (see black line on fragment 3) and measures an angle θ. Next, an interpreter measures of signal propagation velocity V and radius of a cylinder r by means of fitting a hyperbolic curve by interactive varying of these parameters (see fragment 2). In the end the interpreter fixes inclined line by changing φ value to obtain parallel bounds of reflections of the cylinder high generatrix (see fragment 1).

All data entered by the interpreter are displayed in group of operating elements "Cylinder". Meaning of these elements is given in the following list:

Tt—depth of top of an approximating hyperbole measured in time samples;

Width—number of the samples in the approximating hyperbole of a fragment 2;

Theta—value of a corner $\boldsymbol{\theta}$ measured in degrees;

V—propagation speed for of signals measured in millimeters/nanoseconds;

h—depth of cylinder measured on a normal in centimeters;

r—estimation of radius of the cylinder in centimeters;

Phi—value of a corner φ measured in degrees;

Oblique plane—the tag, which passive condition is used at measurements of parameters of horizontal cylinders, and an active condition—at a choice of an inclined secant of a plane in parallel an axis of the cylinder;

Measurement zone—a tag at which installation on a fragment 1 there are vertical borders of the measured length of the cylinder;

St—position of the left border of the cylinder measured in samples of scanning zone;

End—position of the right border of the cylinder measured in samples of scanning zone.

Measured parameters such as coordinates of the measurement point, the propagation velocity and also parameters of a cylindrical object such as radius, length and location are shown in status bar (Fig. 3). Value PSI shows direction of vector h. It equals $PSI = \pi/2 - \varphi$.

Inaccuracy of measurements of unknown parameters depends on next factors: the time discretization, the discrete location of antenna, the size of a object, insufficiently stretched "tails" of hyperbolic reflections restricted by directional diagram, GPR resolution, the small amplitude of reflections and the level of suppression of useful signals by reflections from other objects.

3. Conclusion

An interactive measurement technique developed in this paper allows the use of 3D GPR data which are reflections from a buried cylinder to define the signal propagation velocity in a medium and parameters of a cylindrical object such as radius, length, depth, azimuth angle and angle of inclination can be found.

Parameters which are found can be use both for direct interpretation of observed objects and for automatic shaping of reflecting surfaces of all objects detected in the scan area using the method in [4].

REFERENCES

1. Shihab, S., W. Al-Nuaimy, and A. Eriksen, "Radius estimation for subsurface cylindrical objects detected by ground penetrating radar," *Tenth Intern. Conference on Ground Penetrating Radar*, Delft, The Netherlands, June 21–24, 2004.
2. Al-Nuaimy, W., S. Shihab, and A. Eriksen, "Data fusion for accurate characterisation of buried cylindrical objects using GPR," *Tenth Intern. Conference on Ground Penetrating Radar*, Delft, The Netherlands, June 21–24, 2004.
3. Windsor, C. G., P. Falorni, and L. Capineri, "The estimation of buried pipe diameters by generalized hough transform of radar data," *PIERS 2005*, Haungzhou, China.
4. Yufryakov, B. A., B. S. Surikov, Y. G. Sosulin, and O. N. Linnikov, "A method for interpretation of ground-penetrating radar data," *Journal of Communications Technology and Electronics*, (English Translation of *Radiotekhnika i Elektronika*), Vol. 49, No. 12, 1342–1356, December 2004.
5. Sosulin, Y. G., O. N. Linnikov, B. A. Yufryakov, and V. Y. Bodrov, "Interpretation of ground-penetrating radar data when probing cylinder objects in medium with unknown parameters," *Intern. Radar Symposium IRS 2005*, Germany, Sept. 6–8, 2005.
6. Andryukhin, A. N., O. N. Linnikov, V. N. Trusov, B. A. Yufryakov, V. Y. Bodrov, and Y. G. Sosulin, "Pulse GPR with optoelectronic sensor," *Tenth Intern. Conference on Ground Penetrating Radar*, Delft, The Netherlands, June 21–24, 2004.

Automatic Ground Clutter Rejection Processing Using Doppler-angle Domain Image Features Based Processing (DAIP)

H. Deng
The University of North Texas, USA

For airborne radar systems, the ground clutter received through antenna sidelobe poses a serious threat to effective ground moving target detection. Traditionally Space-Time Adaptive Processing (STAP) is widely used in airborne radar system for ground clutter and jammers. The joint space-time processing is necessary for ground clutter rejection because the ground clutter couples between space domain and time domain due to the platform movement. However, successful implementation of STAP requires accurate estimation of the clutter covariance matrix in real time. The "training" data used for clutter estimation is normally obtained by sampling the secondary units that are spatially adjacent to the primary detection unit with the assumption that the clutters in the primary and secondary units are statistically Independent and Identically Distributed (IID). Since the ground clutter is inhomogeneous in nature, finding sufficient IID secondary data for clutter estimation poses the most serious challenge to successfully implementing STAP algorithm. In this work, a novel Doppler-Angle domain Image feature based Processing (DAIP) technique is to be developed for effective ground clutter rejection processing without using secondary data. The airborne radar system collects the echo data in space-time domain by transmitting multiple coherent pulses and receiving data from each element of an antenna array. STAP suppresses interference by "whitening" interference signals and further integrates target signal through two-dimensional matched filtering in the time-space domain. The proposed DAIP, however, transforms the collected time-space data directly into the Doppler-angle domain; hence, both target signal and interferences are coherently integrated through the transform. The discrimination processing of target and interference signals for target detection is performed based on their different features on the Doppler-angle plane without actually filtering out interference signals.

The target signal is a concentrated point in the transform domain. Jammer signals on the Doppler-angle plane are straight lines parallel to the Doppler axis. Ground clutter on the plane is normally a tilted ridge or even multiple parallel ridges dependent on the ratio of the platform moving speed to the radar Pulse Repetition Frequency (PRF). The thermal noise is statistically uniformly spread in the Doppler-angle plane through the 2-D Fourier transform. Therefore, in the Doppler-angle domain, the structure of target signal is conspicuously different from that of ground clutter or jammer, i.e., target signal is concentrated and interferences are extended. It is further noted that moving target signal generally does not overlap with clutters on the Doppler-angle plane because of their different Doppler frequencies. Hence, based on the above observations DAIP algorithm is to be developed for automatic rejection of ground clutter. The first step of DAIP is to transform radar data collected in the space-time domain to an image in the Doppler-angle domain through two-dimensional Fourier transform. Subsequently, a clamping processing is applied to all pixels of the transformed images to remove the white noise. Following the clamping processing, the remaining non-zero pixels are either target signals or interferences (clutter or jammer). The feature extraction of the clamped image is carried out by clustering non-zero pixels into pixel blocks consisting of consecutively connected non-zero pixels through an image segmentation algorithm called region growing. With the segmentation processing, the image becomes a collection of pixel blocks that are either target or interference. Target detection for a pixel block is based on pixel concentration level, which may be measured by a metric called block size.

The processing results in the work indicate that DAIP can effectively reject ground clutter and detect ground moving targets based on distinguishing features of target and interference in the Doppler-angle domain. Without requirement of estimating clutter covariance, DAIP is particularly suitable for applications in highly inhomogeneous or unknown clutter environment.

InSAR with Multiple Baselines—Comparison of Height Retrieval and Phase Unwrapping Techniques

M. C. Yeung[1], W. D. Wong[1], B.-I. Wu[1], Y. Hara[2], and J. A. Kong[1]

[1]Massachusetts Institute of Technology, USA
[2]Mitsubishi Electric Corporation, Japan

This study investigates both interferometric SAR (InSAR) post processing height retrieval techniques as well as phase unwrapping techniques when we use three satellites (and hence three baselines). Potential advantages of this configuration are explored and compared with the original 2-satellite method. For height retrieval, 3 methods were compared. The first approach is data averaging—3 interferograms retrieved per look are grouped into pairs, with the 2 best selected to be averaged to produce a better estimate of the digital elevation map (DEM). The second approach is the unambiguous range magnification (URM) method, which expands the unambiguous wrapped phase range by taking advantage of the observation that phases for different satellites wrap at different rates because of different distances and geometries relative to the same terrain pixel. Thus, the wrapped phase range is increased multiple fold from 2π without doing any phase unwrapping. This eases the reliance on phase unwrapping when performing height retrieval. The third approach is the maximum likelihood estimator (MLE), which uses URM to predict the closest phase estimate which best fits most of the data sets available.

It is shown that for multiple flyover looks, the data-averaging method is an efficient and computationally inexpensive method to obtain improved retrieved heights. The MLE technique is asymptotically favorable over the data averaging method, which may or may not be the case in a real situation. The URM method performs the worst among the 3, since it relies on the shortest baseline for unwrapping—unfortunately, the shortest baseline is most susceptible to noise.

For 3D phase unwrapping, we introduce the 3D Projection method, which uses the geometry of the satellite configuration to create constraints for the values of the phase differences. Noise, which moves phase points away from the "line segments" which define such constraints, can be filtered out if we manually adjust the phases such that they once again obey the constraints. The results show that this method works better than if such a processing step was not taken.

Effect of Rain on Zenith Path Sky Noise Temperature at 29.9 GHz at Tropical Site Amritsar

P. Sharma
Guru Nanak Dev University, India

I. S. Hudiara
KC College of Engg., India

M. L. Singh
Guru Nanak Dev University, India

Rain has long been recognized as the major and foremost factor that causes fading of wireless communication systems. The effect is dependent on the various factors such as the site (location of the communication link or satellite), frequency of the operation, and of the elevation. The present communication is an abstract from the long term microwave propagation measurement program being going at CRL, GNDU, Amritsar since 2001.

Here the results in the form of rain rate and corresponding variation in sky noise temperature have been presented. The corresponding values of the zenith path attenuation have also been derived.

The rain rate has been measured with tipping bucket type rain guage having resolution 0.254 mm and corresponding sky noise temperature with zenith looking Dicke type radiometer at 29.9 GHz installed at CRL, GNDU, Amritsar, Punjab, India.

Enhanced Detection and Classification of Buried Mines with an UWB Multistatic GPR

A. J. Dumanian
MIT Lincoln Laboratory, USA

C. Rappaport
Northeastern University, USA

We present a resonance-based classification technique for the identification of plastic-cased antipersonnel (AP) land mines buried in lossy and dispersive soils under rough surfaces by a stepped-frequency ultra-wideband (UWB) downward-looking ground penetrating radar (GPR) with an array of receivers. For this application the multistatic ground probing sensor is positioned just above the ground surface and operates from UHF to C-Band frequencies. Novel physics-based models based on the finite difference frequency domain (FDFD) technique simulate the characteristic resonating multi-aspect target frequency responses for several realistic buried land mine detection scenarios. Matched filter detection results are presented which assess the GPR's performance in identifying a simulated mine buried under a rough surface at varying depths in dry sand and a dispersive clay loam soil from other false targets such as buried rocks.

*This work was sponsored by the Department of the Air Force under Air Force Contract No. FA872105-C-0002 and by CenSSIS, the Center for Subsurface Sensing and Imaging Systems under the Engineering Research Centers Program of the National Science Foundation (Award EEC-9986821). Opinions, interpretations, conclusions, and recommendations are those of the author and are not necessarily endorsed by the United States Government.

Electrical Properties of Titan Surface from Cassini Scatterometer and Radiometer Measurements

H. A. Zebker and L. Wye
Geophysics Stanford University, USA

We observe Titan, Saturn's largest moon, using active and passive microwave instruments carried on board the Cassini spacecraft. The 2.2-cm wavelength penetrates the thick atmosphere and provides measurements at resolutions from 10-200 km over much of the moon surface. Here we seek to explain Titan's simultaneous high reflectivity and high emissivity, using a layered model in which a gray body emissive material is overlain by a nearly lossless but complex icy layer. The lossless layer is required to produce the high radar returns through coherent backscattering, while the absorptive substrate is needed to produce high radiative temperatures. We use angle diversity to separate a Hagfors? like surface scattering term from a diffuse volume scattering term in the radar echo, and retrieve dielectric constants ranging 1.5 to greater than 3 for much of the surface. The specular term also yields surface slope distributions from a few degrees rms to greater than 15 degrees in different regions. The reduction of the radiometry data also gives dielectric constants over the same range, but the average properties of Titan favor the lower values. Dielectric constants of 1.7 are indicative of frozen hydrocarbon materials such as methane or ethane, while water ice has a dielectric constant of 3.2. If the surface is composed largely of water ice, it would have to be unconsolidated material such as snow where the bulk electrical properties are reduced by the fractional volume of material. Many small scale features are seen and differ both in emissivity and reflectivity from the average values, and likely give clues to the nature of geologic processes occurring on the surface.

Preliminary Detection of the Dangerous Meteorological Phenomena and Selections Closed Objects by the Help Radar with Variable Polarization

A. B. Shupiatsky
141700 Moscow Region, Dolgoprudny, Russia

The review of theoretical and experimental studies of meteorological events and reflections from ground and structures on it, covered by deposits, fogs and other meteorological object by dual-polarization radars are presented. Theoretical and experimental foundations of the polarization methods of detecting dangerous weather phenomena are made. Theoretical models of polarization characteristics (linear and elliptical) of radar signals from different kinds of clouds and precipitation are worked out and described. From common case of elliptically polarization is shows sensibility echo signal from microstructure of reflected particles. A choice of optimal polarization may by make.

Algorithms of the detection of a variety of hydrometeors and optimal polarization are discussed. Creation of algorithms of connection of microstructure and dangerous weather phenomena with polarization characteristics of radar signals are presented. Requirements to the equipment and up-dating of existing radars are formulated. These algorithms and requirements were realized on basis of polarization airborn and ground dual-polarization weather radars. These diversity-polarization radar are described.

Methods and means for remote detection of pre-storm state, increased electrical activity, zones of icing , hail and shower clouds, heavy precipitation, turbulence and other weather phenomena and conditions which are dangerous for flights of air vessel and human activities. It is necessary to note one more important developed direction in polarizing radiometeorology. It is a bistatic mode of reception of signals. With this mode considerably extends information of the polarizing characteristics of a signal. Theoretically and experimentally is shown, that with reception of signals not only with a return corner of dispersion of 180 degrees, but also in a general case with other corners of dispersion, volume of the information about reflecting object considerably extends. So from the point of view of meteorological tasks the detection of large particles in a cloud, spectrum of their distribution, phase structure is possible. The theoretical substantiation developed a technique and the equipment for realization of this mode of operations is resulted.

The prospects of application SAR in radiometeorological researches are discussed. One of the basic advantages of such aerials are an opportunity to operate the form of the diagram of a direction, to form some diagrams of the various form, that is very important with sounding volumetric diverse meteorological objects. Thus the high speed of scanning, opportunity of adaptation to varying external conditions for example, formation of failures on interfering reflections, opportunity is reached many functional of use, that is simultaneous maintenance of search, detection and support of various objects. So, the application of SAR in meteorological researches allows:

1. Quickly to translate the diagram of a direction from one part meteorological object on other or on other close located object, that is very important for comparison with evolution of a cloud especially with artificial influences.
2. Opportunity of adaptation to quickly varying conditions.
3. It is essential to raise resolution in space.
4. To operate during supervision the form of the diagram of a direction and quantity petals of it, that allows to minimize unnecessary reflections and to allocate researched object.

There are also other important qualities of use of SAR in meteorology. However these aerials are complex and also main while expensive for meteorological researches. Nevertheless progress in development and use of such aerials is obvious.

Apparently Abnormal Satellite Thermal Signals of Infrared Band as a Thermal Plateau on the Sea Surface

S. Nakamura
Kyoto University-Retired/Geophysical Advisor, Japan

The author has had studied about the thermal pattern as a thermal plateau or a pinnacle which was obtaibed by a directly monitoring of the satellite signals. A dynamical model is introduced for realizing this thermo plateau on the sea surface. A supporting thermal pattern is shown as well as the related meteorological data.